Crystal structure of inositol polyphosphate 1-phosphatase at 2.3-A resolution.

ARTICLE *in* BIOCHEMISTRY · DECEMBER 1994

Impact Factor: 3.02 · Source: PubMed

5 AUTHORS, INCLUDING:

Jay Ponder
Washington University in St. Louis
57 PUBLICATIONS **7,215** CITATIONS
SEE PROFILE

Francis Scott Mathews
Washington University in St. Louis
192 PUBLICATIONS **14,744** CITATIONS
SEE PROFILE

Accelerated Publications

Crystal Structure of Inositol Polyphosphate 1-Phosphatase at 2.3-Å Resolution[†,‡]

John D. York,[*,§] Jay W. Ponder,[∥] Zhi-wei Chen,[∥] F. Scott Mathews,[∥] and Philip W. Majerus[§]

Division of Hematology/Oncology and Department of Biochemistry and Molecular Biophysics, Washington University School of Medicine, St. Louis, Missouri 63110

Received July 20, 1994; Revised Manuscript Received September 14, 1994[⊗]

ABSTRACT: Bovine inositol polyphosphate 1-phosphatase (1-ptase), M_r = 44 000, is a Mg^{2+}-dependent/Li^+-sensitive enzyme that catalyzes the hydrolysis of the 1-position phosphate from inositol 1,4-bisphosphate and inositol 1,3,4-trisphosphate. We have determined the crystal structure of recombinant bovine 1-ptase in the presence of Mg^{2+} by multiple isomorphous replacement. The structure is currently refined to an R value of 0.198 for 15 563 reflections within a resolution range of 8.0−2.3 Å. 1-Ptase is monomeric in the crystal, consistent with biochemical data, and folds into an alternatively layered $\alpha/\beta/\alpha/\beta$ sandwich. The central core of 1-ptase consists of a six-stranded antiparallel β sheet perpendicular to two parallel three-turn α-helices. The β sheet is flanked by two antiparallel six-turn α-helices aligned parallel to the β sheet, and the central helices are flanked by a five-stranded largely parallel β sheet. Two neighboring metal binding sites are located in adjacent acidic pockets formed by the intersection of several secondary structure elements including an unusual kink structure formed by the "DPIDST" sequence motif. The fold of 1-ptase is similar to that of two other metal-dependent/Li^+-sensitive phosphatases, inositol monophosphate phosphatase and fructose 1,6-bisphosphatase despite minimal amino acid identity. Comparison of the active-site pockets of these proteins will likely provide insight into substrate binding and the mechanisms of metal-dependent catalysis and Li^+ inhibition.

Agonist-induced phosphatidylinositol turnover is mediated by phospholipase C hydrolysis of phospholipids to yield diacylglycerol, inositol phosphates, and cyclic inositol phosphates (Majerus, 1992). Roles in intracellular signaling have been well documented for diacylglycerol (Nishizuka, 1986) and inositol 1,4,5-trisphosphate (Berridge, 1989). The actions of inositol phosphate phosphatases and kinases give rise to a plethora of inositol polyphosphates that may also serve as signaling or regulatory molecules (Bansal & Majerus, 1990). Roles for other inositol phosphates and cyclic inositol phosphates have also been proposed (Majerus, 1992; Bansal & Majerus, 1990; Berridge, 1989); however, the functions of most inositol polyphosphates remain unknown.

Inositol polyphosphate 1-phosphatase (1-ptase) removes the 1-position phosphate from inositol 1,4-bisphosphate [Ins(1,4)P_2] and inositol 1,3,4-trisphosphate [Ins(1,3,4)P_3], yielding inositol 4-phosphate and inositol 3,4-bisphosphate, respectively (Inhorn & Majerus, 1987, 1988; Gee et al., 1988). 1-Ptase is a ubiquitous monomeric enzyme that requires Mg^{2+} for activity and is potently inhibited by Li^+ and Ca^{2+} ions. Cell fractionation and immunolocalization studies of endogenous and transiently expressed recombinant 1-ptase have shown that it is concentrated in the nucleus (York et al., 1994a) despite the absence of a canonical nuclear targeting sequence (Dingwall & Laskey, 1991; Silver, 1991). In addition, COS 7 and HeLa cells transiently overexpressing 1-ptase show a diminution of DNA synthesis while overexpression of a catalytically inactive 1-ptase has no effect on DNA synthesis, thereby suggesting that a substrate or product is involved in the modulation of DNA synthesis (York et al., 1994a). These data are consistent with a proposed signaling role for Ins(1,4)P_2 in which it binds to and stimulates the activity of DNA polymerase α *in vitro* (Sylvia et al., 1988).

The sequence of 1-ptase is highly conserved between cow and human (York, 1990, 1993) but does not show obvious sequence homology with other proteins in the GenBank database. However, two short sequence motifs, WVDP(I/L)D(G/S)T (residues 151−158 in 1-ptase) and WDXXAILXXAGG (residues 316−330 in 1-ptase), are present in several proteins including mammalian inositol monophosphate phosphatase (m-ptase), *Escherichia coli* SuhB and AmtA, and fungal Qa-X and QutG (York, 1990; Neuwald, 1991). m-Ptase is a Mg^{2+}-dependent/Li^+-sensitive phosphatase that removes the phosphate from all equatorial monophosphorylated inositols to yield inositol (Hallcher & Sherman, 1980), while the function of the other proteins is not well understood. The crystal structure of m-ptase, determined at 2.1-Å resolution (Bone et al., 1992), demon-

[†] This research was supported by Grants HL 14147 (Specialized Center for Research in Thrombosis), HL 16634, HL 07088, GM 24483-14, and GM 20530 from the National Institutes of Health.

[‡] The coordinates for the crystal structure of inositol polyphosphate 1-phosphatase have been deposited with the Brookhaven Protein Data Bank under the filename 1inp.

* Address correspondence to this author at the Division of Hematology/Oncology, Washington University School of Medicine, Box 8125, 660 S. Euclid Ave., St. Louis, MO 63110 [phone, (314) 362-8825; Fax, (314) 362-8826; E-mail, york@visar.wustl.edu].

[§] Division of Hematology/Oncology.

[∥] Department of Biochemistry and Molecular Biophysics.

[⊗] Abstract published in *Advance ACS Abstracts,* October 15, 1994.

0006-2960/94/0433-13164$04.50/0

strates that highly conserved residues within these motifs are important for metal binding and catalytic function.

We have previously reported the isolation and initial crystallographic parameters of recombinant bovine 1-ptase produced using a baculovirus expression system (York et al., 1994b). In the present study, we have solved the three-dimensional structure of 1-ptase in the presence of Mg^{2+} by multiple isomorphous replacement (MIR) at 2.3-Å resolution. The structure of 1-ptase is similar to two other metal-dependent phosphatases, m-ptase (Bone et al., 1992) and fructose 1,6-bisphosphatase (fb-ptase) (Ke et al., 1989).

EXPERIMENTAL PROCEDURES

Crystallization and Heavy Atom Derivative Preparation. Tetragonal-shaped crystals suitable for diffraction with dimensions routinely exceeding 0.2 × 0.2 × 1.0 mm were obtained as previously described (York et al., 1994b). Briefly, crystals were grown by hanging-drop vapor diffusion on silanized glass cover slips at 20 °C using 3 μL of 13 mg/mL pure recombinant bovine 1-ptase in 10 mM Bis-Tris, pH = 6.3, and 3 mM $MgCl_2$ plus 3 μL of 13% PEG-8000, 200 mM Li_2SO_4, and 100 mM Tris, pH = 6.3 (liquor A), and equilibrated with a reservoir of 500 μL of liquor A. Crystals reached maximum size after 5−7 days and were stable for at least 6 months. Heavy atom derivatives were prepared by adding 0.5 μL of 42 mM $GdCl_3$, 17.5 mM $Gd_2(SO_4)_3$, or 7 mM ethylmercuriothiosalicylic acid (EMTS) in liquor A to 3-μL hanging drops containing native crystals for 1−2 days.

Data Collection and Heavy Atom Phasing. Crystals were mounted in 0.7-mm quartz capillaries, and diffraction data were measured at 4 °C by ω scans on dual Xuong-Hamlin Mark II multiwire area detectors (Hamlin, 1985) equipped with helium boxes at detector to crystal distances of 880 and 835 mm. Cu Kα X-rays were generated by a Rigaku RU200 rotating anode equipped with a Supper graphite monochromator operating at 50 kV and 150 mA. Data for native and heavy atom derivatives were typically collected as high- and low-resolution data sets on a single crystal with θ_c values ranging from 30° to 13°. Collection strategies were determined as described by Xuong and colleagues (Xuong et al., 1985) in which ω was incremented in 0.1° frames at a rate of 25 s per frame (15 s per frame for low-resolution data). Intensity data reduction, merging, and scaling were performed using the area detector software (Howard et al., 1985). Anomalous data sets were collected on heavy atom derivatives by complementing original ϕ, χ orientations with $\phi + 180°$, $-\chi$ orientations. Data from these sets were reduced without merging Bijvoet pairs. During the search for heavy atom derivatives we encountered several derivatives that resulted in R_{ISO} ($\sum||F_{derivative}| - |F_{native}||/\sum|F_{native}|$) values above 0.4. We were able to correct this problem inherent to crystals having a point group of *P*4 in which the physical orientation of the crystal along the C axis is critical for proper indexing. By simple reassignment of *h,k,l* to *h,*−*k,*−*l*, R_{ISO} factors dropped below 0.2. (We thank Dr. Arthur Arnone at the University of Iowa for this critical suggestion.) Heavy atom insertion sites were determined from difference Patterson functions and were identical to those obtained from anomalous difference Pattersons. Binding parameters were refined iteratively using "HEAVY" (Terwilliger et al., 1987) until position, occupancy, and temperature factors converged (typically five cycles).

MIR-including anomalous scattering (MIRAS) phases were calculated from native and heavy atom derivative data sets, including anomalous difference data, using the program LSM4PH (Mathews et al., 1972). The program was repeatedly run, each time updating isomorphous and anomalous closure errors, until these values converged (typically four cycles). The anomalous scattering contribution of the Gd^{3+} derivative was used to determine the absolute conformation of the molecule (Blundell & Johnson, 1976). MIRAS phases were improved by solvent-flattening and histogram-matching algorithms and extended to 2.3 Å using SQUASH (SQ-MIRAS) (Zhang & Main, 1990; Zhang, 1993). In order to minimize loss of surface density information, the solvent content used in solvent-flattening calculations was 35%, well below the estimated 43% crystal solvent content (York et al., 1994b).

Model Building and Refinement. Initial α-carbon positions were traced from 3.0-Å and 2.3-Å SQ-MIRAS electron density maps. Minimaps were used to approximately place coordinates after which they were repositioned using TURBO (Cambillua & Horjales, 1987) on a Silicon Graphics Indigo workstation. The initial trace contained several discontinuous regions confined to surface loops which prevented complete sequence assignment. Backbone and side-chain atoms were built from α-carbon coordinates using "O" (Jones et al., 1991). The partial model was refined within a resolution range of 10−3 Å using X-PLOR (Brünger, 1988) and manually refit to SQ-MIRAS density maps. Each round of refinement consisted of positional refinement, simulated annealing (3000−300 K, time step of 0.0008 ns), and individual isotropic temperature factor refinement procedures. The remaining loop regions were traced with the aid of the BONES skeletonizing subroutine (Jones, 1985) from either $(2F_o - F_c)\alpha_c$, where F_o and F_c are defined as the observed native and calculated model-based structure factors, and maps or "combined" maps in which model-based phases were combined with MIRAS phases (Read, 1986; Agarwal, 1978; Zhang, 1993). The complete model was improved by several rounds of refinement and fitting. After each round the resolution was gradually increased until it reached 2.3 Å. Temperature factors were refined each round in order to calculate density maps; however, they were not retained for each subsequent round until the last rounds when the resolution limit was 2.3 Å. Water molecules were added in steps at positions showing density peaks $\geq 3.5\sigma$ in $(F_o - F_c)\alpha_c$ maps and having acceptable hydrogen-bonding geometry. The structure including water molecules was refined by positional refinement and individual isotropic temperature factor refinement.

The 1-ptase/Gd^{3+} model was obtained by refinement of 1-ptase model VI coordinates including both metal ions but excluding solvent using Gd^{3+} structure factors. A single round of simulated annealing (1000−300 K, time step of 0.001 ns) was performed, omitting an 8.0-Å sphere surrounding metal sites 1 and 2. A 3-Å cushion surrounding these spheres was constrained to prevent movement of protein atoms into the electron density of the omitted region. $2F_o - F_c$ omit maps were generated, and the model was repositioned manually into density in the omitted region. This final 1-ptase/Gd^{3+} model was generated by positional and individual isotropic temperature factor refinement, followed by placement of solvent molecules within 10 Å of metal sites. Superimposition of structures by a least-squares method was

Table 1: Statistics for X-ray Diffraction Data

	native	EMTS		$GdCl_3$	$Gd_2(SO_4)_3$	
data set name	ptnat-hl	em03	em4r	gd1r	gd2r	gd04
soaking conditions (mM, h)		1, 48	1, 23	6.0, 48	2.5, 72	2.5, 48
no. of sites		2	4	1	1	1
R_{ISO}[a]		0.164	0.160	0.126	0.120	0.117
resolution limit (Å)	2.3	3.0	3.6	3.2	3.0	2.5
no. of observations	63687	28749	29123	21164	23742	88475
no. of unique	17652	7820	9355[b]	6169	7413	26197[b]
% completeness	99.3	93.9	96.8	91.5	90.1	96.0
av $I/\sigma(I)$	10.5	5.1	9.9	7.3	8.0	10.8
av decay/ reflection[c] (%)	36	42	44	13	22	37
R_{SYM}[d]	0.049	0.087	0.046	0.072	0.070	0.051

[a] $R_{ISO} = \sum||F_{derivative}| - |F_{native}||/\sum|F_{native}|$. [b] Bijvoet pairs were unmerged. [c] Average decay was determined by comparing intensities of identical reflection sets at the beginning and end of the data collection. [d] $R_{SYM} = \sum|I(av - obs)|/\sum I(av)$.

performed using the program INSIGHT II. m-Ptase and fb-ptase PDB coordinate files used for superimposition were obtained from the Brookhaven Database under the file names 2hhm.pdb and 1fbp.pdb.

RESULTS

Structure Solution of Recombinant Bovine 1-Ptase. Recombinant bovine 1-ptase formed crystals suitable for diffraction studies at 2.3-Å resolution. Crystallographic parameters were previously determined to be $a = b = 51.64$ Å, $c = 143.33$ Å, $\alpha = \beta = \gamma = 90°$ in a space group of $P4_1$ or $P4_3$ (York et al., 1994b). A single native 1-ptase crystal grown in the presence of Mg^{2+} was used to collect a data set that was 99% complete within a resolution range of 20–2.3 Å. We initiated a search for heavy atom derivatives in order to solve the structure by MIR, and two compounds, Gd^{3+} and EMTS, yielded useful isomorphous derivatives. Diffraction data, in some cases including anomalous differences, were collected from multiple crystals of each derivative; the statistics are summarized in Table 1. Difference Patterson maps between the native and derivative data showed a single Gd^{3+} site and one to two major EMTS sites, depending on the crystal. These positions were refined, and difference Fourier analysis was used to verify the sites and to identify additional low-occupancy sites. One or two additional EMTS sites were identified while no additional Gd^{3+} sites were found. The refined sites for the heavy atom derivatives are shown in Table 2.

Phasing was initially tried to 3.0-Å resolution using native and both EMTS derivative data sets including anomalous data. However, the figure of merit (FOM) was below 0.5, and the electron density map was uninterpretable. Single isomorphous replacement phases were then calculated using the Gd^{3+} derivative gd04, which included anomalous differences to yield an average FOM of 0.66 to 3.0-Å resolution. MIRAS phases were then calculated using all data sets, including anomalous data, with an overall FOM of 0.72 to 3.0-Å resolution and 0.63 to 2.5-Å resolution. The correct configuration of the protein was determined to be $P4_1$ by comparison of difference Fourier peaks calculated using the Gd^{3+} phases along with anomalous contributions and both arrangements of EMTS atoms. MIRAS phases were used to calculate a 3.0-Å electron density map which showed distinct secondary structure elements; however, molecular

Table 2: Refined Heavy Atom Derivatives

derivative	data set	site	X	Y	Z	occ[a]	B[b]	phasing power[c]
$GdCl_3$	gd1r	1	0.309	0.172	0.000	0.078	44.30	1.14
$Gd_2(SO_4)_3$	gd2r	1	0.309	0.172	0.000	0.081	48.72	1.23
	gd04	1	0.306	0.172	0.000	0.069	32.90	1.37
EMTS	em03	1	0.008	0.398	0.025	0.062	60.22	0.77
		2[d]	0.083	0.033	0.051	0.018	25.77	
	em4r	1	0.008	0.400	0.022	0.045	35.10[e]	0.98
		2[d]	0.074	0.042	0.051	0.024	35.10[e]	
		3[d]	0.346	0.499	0.467	0.020	35.10[e]	
		4[d]	0.044	0.084	0.035	0.021	35.10[e]	

[a] Relative occupancy as described by the program HEAVY (Terwilliger et al., 1987). [b] Isotropic temperature factor. [c] Phasing power is defined as the RMS heavy atoms structure factor divided by the RMS isomorphous lack of closure error. [d] Low occupancy sites were identified using isomorphous difference Fourier and the gd04 phases. [e] Temperature factors were not refined.

Table 3: 1-Ptase Refinement Statistics

model[a]	no. of atoms protein[b]	no. of atoms solvent/Mg^{2+}	resolution range (Å)	$R_{initial}$[c]	R_{final}[c]
I	2720	0	10.0–3.0	0.434	0.236
II	3088	0	10.0–3.0	0.265	0.216
	3088	0	10.0–2.7	0.267	0.238
III	3088	0	8.0–2.5	0.257	0.231
	3088	0	8.0–2.3	0.283	0.217
IV	3088	42/2	8.0–2.3	0.225	0.205
V	3088	58/2	8.0–2.3	0.207	0.200
VI	3088	69/2	8.0–2.3	0.203	0.198
1pt/Gd^{3+}	3088	8/2	8.0–2.5	0.280	0.198

[a] Model I, partial model containing 355 residues out of 400 which was fit to a 3.0-Å SQ-MIRAS map; model II, complete model fit to a 3.0-Å SQ-MIRAS map; model III, fit to a 2.5-Å SQ-MIRAS map and then the refined 2.5-Å model fit to a 2.3-Å $(2F_o - F_c)\alpha_c$ map; models IV–VI, gradual introduction of water and metal ions and fitting to 2.3-Å $(2F_o - F_c)\alpha_c$ maps; model 1pt/Gd^{3+}, 1-ptase/Gd^{3+} derivative structure factors. [b] Excludes hydrogen atoms. [c] Standard R factor defined by $\sum|F_o - kF_c|/F_o$.

boundaries were not clearly demarcated. MIRAS phases were improved using the SQUASH solvent-flattening and histogram-matching routines which gave average FOM values of 0.87, 0.84, and 0.76 for 20.0–3.0-, 2.5-, and 2.3-Å resolution limits, respectively.

Initially, the 1-ptase structure was traced using two electron density maps calculated from SQ-MIRAS phases at 3.0- and 2.3-Å resolution. The boundaries of the molecule were clearly visible and allowed the placement of 355 residues out of a total of 400, yielding three discontinuous polypeptide chains spanning residues 1–233, 263–275, and 284–392. Sequence assignments were made on 330 of these residues on the basis of unambiguous side-chain density or continuous peptide chains, which were flanked by several "signature" residues, i.e., TYR, TRP, PHE, or HIS. The remaining 25 unassigned residues were built as alanine. The incomplete model was refined (Table 3) and then used to generate $(2F_o - F_c)\alpha_c$ maps and combined maps. The remaining 45 residues were traced using these maps. Several loop regions were disordered and had to be traced through density at less than 1σ contour levels. Density at this contour often contained branches which were resolved with the aid of the BONES skeletonizing program.

The complete model was refined and manually refit in several steps as summarized in Table 3. Each round of refinement typically consisted of positional refinement,

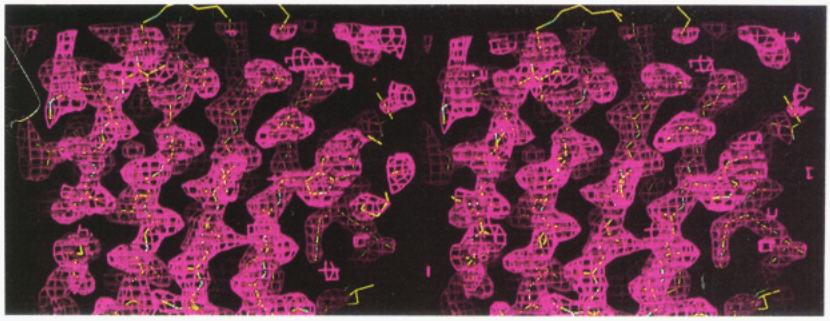

FIGURE 1: Stereo image of 1-ptase fitted to electron density. A stereoview of a $(2F_o - F_c)\alpha_c$ 2.3-Å electron density map surrounding the central β-sheet region including strands β4, rightmost, to β8 (see text for residue numbers) is shown at a contour level of 2σ.

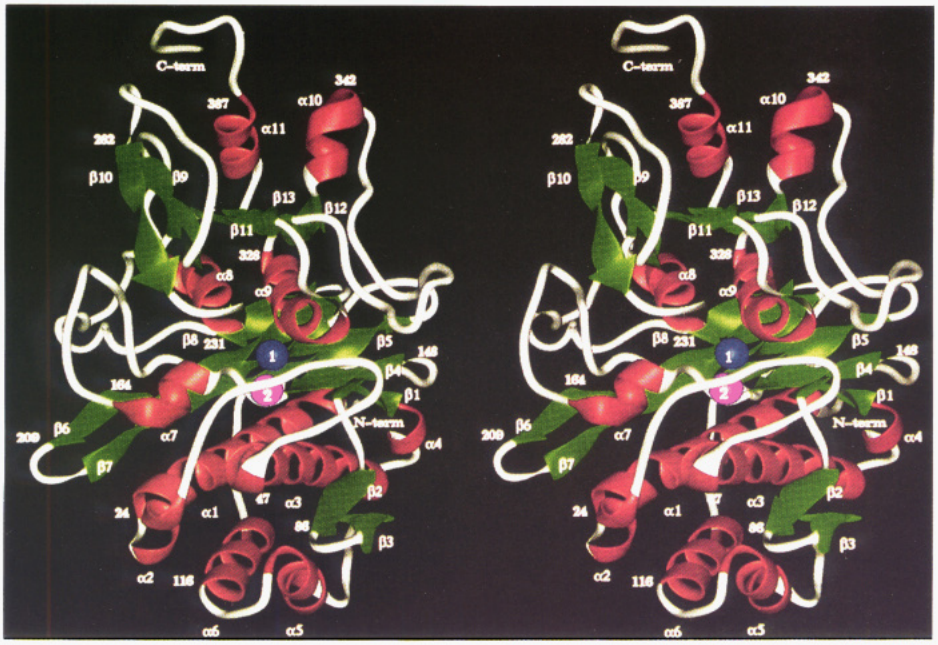

FIGURE 2: Structure of inositol polyphosphate 1-phosphatase. Stereoview of the 1-ptase ribbon drawing generated from the final refined coordinates, model VI, as stylized using the MIDAS "cartoon". Secondary structure elements are defined essentially as described (Kabsch & Sander, 1983), labeled sequentially, and colored to emphasize α and β layers. β strands are green, α-helices are red, and coiled regions are white. Selected residues are numbered and the N and C termini are labeled. Mg^{2+} binding sites 1 and 2 are shown as dark blue and magenta spheres, respectively.

simulated annealing, and individual isotropic temperature factor refinement using X-PLOR. Water and metal molecules were conservatively added and refined as above except that simulated annealing was omitted. The final structure has a conventional R factor of 19.8% for 15 563 unique reflections between 8.0 and 2.3 Å with $F > 2\sigma$. The root mean squared (RMS) deviations from ideality for the bond lengths, angles, dihedrals, and improper dihedrals are 0.016 Å, 3.55°, 26.03°, and 1.31°, respectively. The electron density map calculated from model VI, $(2F_o - F_c)\alpha_c$, shows strong, well-defined density as shown in Figure 1. The final coordinates contain 11 Ramachandran plot outliers (data not shown) which are confined to loop regions of weak density. The average overall temperature factor is 36.28 Å^2. The relatively high average is due to several surface loop regions having temperature factors above 60.0 Å^2. The 307 residues with temperature factors below 60.0 Å^2 have an average of 24.85 Å^2. One cis peptide bond is present between ASP 133 and PRO 134 despite several attempts during refinement to fit the peptide bond into the trans conformation.

1-Ptase Structure. The structure of 1-ptase is a single cylindrical domain, approximately 50 Å in diameter and 80 Å long, composed of several layers of α-helices and β sheets as shown in Figure 2. A total of 11 α-helices and 13 β strands make up six distinct layers. The first layer, starting from the bottom in Figure 2, consists of two antiparallel two- and three-turn helices (α5, GLU 102−LEU 111, and α6, LEU 116−GLN 127) which form a helical bundle with the two antiparallel six-turn helices (α1, ASP 3−GLN 24, and α3, VAL 47−LYS 68) in the second layer. The C termini of both helices, α1 and α3, are capped by a single-turn helix (α2, GLU 26−LEU 31, and α4, LEU 72−LYS 75) oriented at 90° angles. The third layer is a large six-stranded antiparallel β sheet (β1, LYS 75−GLU 79, β4, LEU 148−ASP 153, β5, VAL 182−ASP 190, β6, LEU 197−ASP 209, β7, ARG 213−SER 224, and β8, GLY 227−231 HIS) oriented in parallel with the second helical layer. This layer also contains an unusual "kink" structure (ASP 153−THR 158) which extends into a single-turn helix (α7, TYR 159−GLY 164). Two three-turn parallel helices (α8, ALA 291−GLY 301, and α9, PHE 314−MET 328) are aligned perpendicular to the β sheet to form the fourth layer. The fifth layer is made up of a largely parallel five-stranded β sheet (β9, SER 262−SER 268, β10, GLY 282−ALA 288, β11, ASP 304−SER 309, and β12, GLY 330−ASP 334 are parallel, while β13, GLY 372−ARG 377, positioned spatially

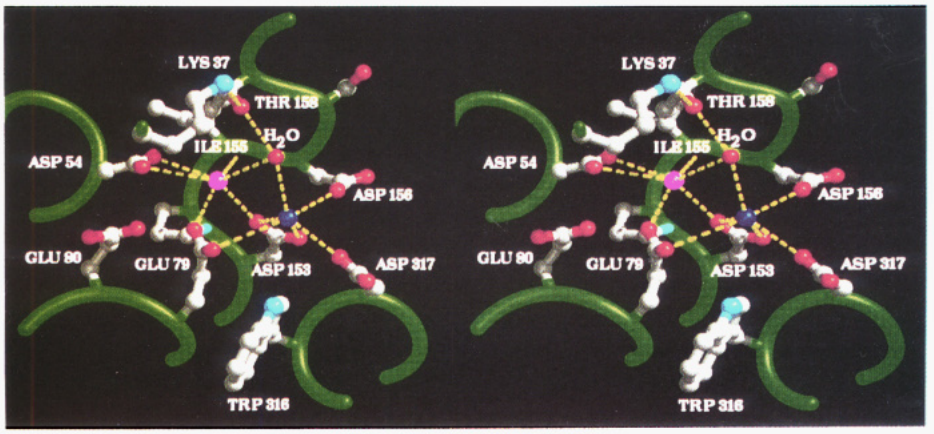

FIGURE 3: Magnesium binding site of 1-ptase. Stereoview of adjacent Mg^{2+} binding sites located at the intersection of four secondary structural elements. Two individual sites were determined by difference Fourier calculated using native structure factors and refined coordinate structure factors and phases. Mg^{2+} binding sites 1 and 2 and H_2O 45 are shown as dark blue, magenta, and red spheres, respectively. The distance between site 1 and site 2 is 3.88 Å. Coordinating ligand distances for site 1 are GLU 79 OE2, 3.8 Å; ASP 153 OD1 and OD2, 3.13 and 3.24 Å; ASP 156 OD2, 3.28 Å; ASP 317 OD1, 3.14 Å; H_2O 45 O, 3.35 Å. These distances for binding site 2 are ASP 54 OD1 and OD2, 3.47 and 3.54 Å; GLU 79 OE1, 2.63 Å; ILE 155 O, 2.48 Å; H_2O 45 O, 3.91 Å. In addition, potential hydrogen bonds are shown between THR 158 and H_2O 45 (2.86 Å) and between THR 158 and LYS 37 (3.05 Å).

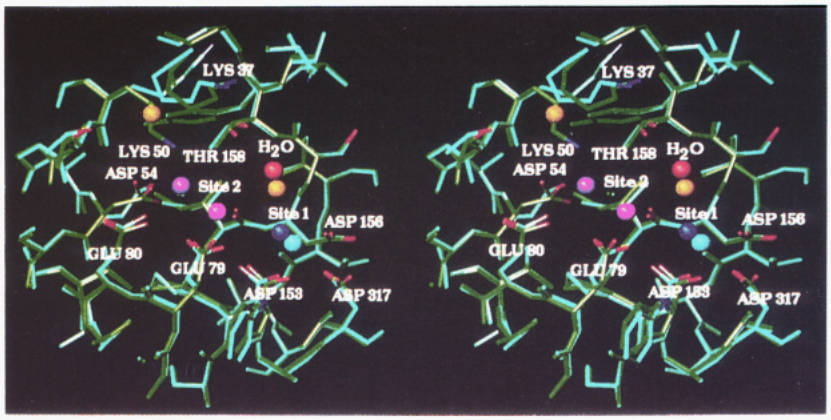

FIGURE 4: Gadolinium metal binding site. Stereoview of superimposed 1-ptase and 1-ptase/Gd^{3+} models surrounding the metal binding sites. Superimposition of residues 1−400 of these models yielded a RMS of 1.020 Å for all non-hydrogen protein atoms and 0.753 Å for α-carbons. RMS deviations for residues surrounding metal binding sites, including residues 54, 79, 80, 153−158, 316, and 317, are 0.524 Å for all atoms and 0.208 Å for α-carbons. 1-Ptase model VI protein atoms are colored green, metal sites 1 and 2 are colored dark blue and magenta, and H_2O 45 is colored red. 1-Ptase/Gd^{3+} protein atoms are colored cyan, metal sites 1 and 2 are colored blue and purple, and water molecules are colored yellow. Side-chain oxygen and nitrogen atoms of selected residues of both models are colored red and dark blue.

between β11 and β12, is oriented antiparallel). Two short helices (α10, LEU 335−ASN 342, and α11, GLU 379−SER 387) pack against each other and the fifth layer β sheet to form a sixth layer.

Metal Binding Sites. Two Mg^{2+} binding sites, site 1 and site 2, are present in the structure of 1-ptase located in adjacent acidic pockets at the intersection of four secondary structure elements, α3, β1, "kink", and α9, as shown in Figure 3. These sites are located in a hydrophilic cavity near the surface of the molecule (see Figure 2). Both sites appear as difference Fourier peaks calculated using native structure factors and model-based structure factors and phases. These peaks were distinguished from solvent molecules by the concentration of surrounding carboxylate groups which form two slightly distorted octahedral coordination pockets, consistent with the expected coordination of Mg^{2+} (Huheey, 1978). Coordinating ligands for Mg^{2+} site 1 (blue in Figure 3) include GLU 79 OE2, ASP 153 OD1 and OD2, ASP 156 OD2, ASP 317 OD1, and H_2O 45 O and for Mg^{2+} site 2 (magenta in Figure 3) include ASP 54 OD1 and OD2, GLU 79 OE1, ILE 155 O, and H_2O 45 O. The distance between metal binding sites is 3.88 Å. 1-Ptase is thought to have two or more cooperative Mg^{2+} binding sites on the basis of a Hill coefficient of 1.9 for the Mg^{2+} dependence of 1-ptase activity (Inhorn & Majerus, 1988).

In order to determine whether or not the metal binding region of 1-ptase was altered by the presence of inhibitory Gd^{3+}, the 1-ptase model was refined using the structure factors from the 1-ptase/Gd^{3+} crystal. Maps omitting residues surrounding the metal binding sites showed clear, well-ordered density. The structure, including Gd^{3+} and 11 solvent molecules surrounding the Gd^{3+} binding site, refined to an R value of 0.19 for 12 001 reflections within a resolution range of 8.0−2.5 Å (Table 3). The 1-ptase/Gd^{3+} model was superimposed onto the 1-ptase model VI, and the region surrounding the metal binding sites is shown in Figure 4. The binding of Gd^{3+} did not cause significant conformational changes within the core structural elements. The backbone atoms of the "DPID" kink surrounding metal site 1 expanded slightly, and the carboxylate of GLU 79 moved inward. Significant changes occurred in the position of metal site 2 and the orientations of neighboring side

Table 4: Superimposition of 1-Ptase, m-Ptase, and fb-Ptase

core structure residues superimposed (α-carbon)[a]	RMS deviation (Å)
1-ptase model VI vs 1pt/Gd^{3+}	0.228
1-ptase model VI vs m-ptase:2hhm[b]	1.478
1-ptase/Gd^{3+} vs m-ptase:2hhm	1.483
1-ptase model VI vs fb-ptase:1fbp[c]	2.659
m-ptase:2hhm vs fb-ptase:1fbp	2.163

[a] The core structure includes the following residues: 1-ptase, α1: 3−23, α3:52−67, β1:74−81, β4:148−158, α7:159−164, β5:181−190, β6:195−205, β7:217−223, β8:228−233, β9:263−268, β10:283−290, α8:291−301, β11:304−308, α9:312−328, β12:329−334, β13:372−377; m-ptase, 7−27, 45−60, 65−72, 85−95, 96−101, 104−113, 116−126, 128−134, 136−141, 157−162, 188−195, 196−206, 209−213, 215−231, 232−237, 249−254; fb-ptase, 28−48, 72−87, 92−99, 113−123, 124−129, 131−140, 158−168, 171−177, 178−183, 207−212, 240−247, 248−258, 260−264, 275−291, 292−297, 315−320. [b] 2hhm was the structure determined in the presence of Gd^{3+} and SO_4 (Bone et al., 1992). [c] The 1fbp structure was determined in the presence of adenine monophosphate, fructose 6-phosphate, and Mg^{2+} (Ke et al., 1989).

chains. While difference Patterson maps showed a single high-occupancy Gd^{3+} binding site with coordinates nearly identical to those of Mg^{2+} site 1, difference Fourier maps showed a second low-occupancy Gd^{3+} site which was shifted 2.75 Å from Mg^{2+} metal site 2. This shift was accompanied by rotation of LYS 50 180° about χ_2 and addition of a well-ordered water molecule. In addition, difference Fourier maps of the 1-ptase/Gd^{3+} model showed a strong density peak surrounding H_2O 45, indicating that binding of Gd^{3+} increases the order of the water or possible replacement of the water by sulfate ion.

Superimposition of 1-Ptase, m-Ptase, and fb-Ptase. The presence of the metal binding motif DPIDST in 1-ptase, m-ptase, and fb-ptase and the fact that all three enzymes are metal-dependent/lithium-sensitive phosphatases suggested that they may be structurally related. The coordinates of the refined 1-ptase model VI were used to compare the 1-ptase structure with those of m-ptase (2hhm.pdb) and fb-ptase (1fbp.pdb). We first superimposed the coordinates for the DPIDST metal binding motif common to the three proteins. RMS deviations of the α-carbons for these six residues of 1-ptase vs m-ptase, 1-ptase vs fb-ptase, and m-ptase vs fb-ptase are 0.602, 0.269, and 0.539 Å, respectively. From these superimpositions we identified a common core structure comprised of 155 residues which form 5 α-helices and 11 β strands. The results of the superimpositions of the core structures are shown in Table 4.

DISCUSSION

Comparison of the structure of 1-ptase with those in the Brookhaven Protein Data Bank showed that it has an identical fold to two other metal-dependent/Li^+-sensitive phosphatases, m-ptase and fb-ptase. The crystal structures of m-ptase and fb-ptase have been determined (Bone et al., 1992; Ke et al., 1989), and recent comparisons of their structures (Liang et al., 1993; Zhang et al., 1993) indicate that they are members of the same structural family despite minimal amino acid identity. The fold of 1-ptase, m-ptase, and fb-ptase consists of alternating layers of α-helices and β sheets which form a core α/β/α/β sandwich. The core structural elements for 1-ptase, as labeled in Figure 2, include α-helices α1, α3, and α7−α9 and β strands β1 and β4−β13, which when aligned with equivalent elements in m-ptase and fb-ptase superimpose with RMS deviations of 1.5 and 2.7 Å. The metal binding sites of all three proteins are structurally conserved and are located at the intersection of several topologically equivalent secondary structure elements.

There are several notable differences among the three proteins. 1-Ptase is a monomer, m-ptase is a homodimer, and fb-ptase is a homotetramer. Arginine residues from adjacent subunits of both m-ptase and fb-ptase project into the active-site pockets and play a role in substrate binding. fb-Ptase is allosterically inhibited by AMP, which binds between N-terminal helices (Ke et al., 1989; Liang et al., 1993). 1-Ptase and m-ptase lack this regulation and do not contain the corresponding amino-terminal helix required for binding of AMP. 1-Ptase contains an additional 50 residues that form a helical layer (layer 1, Figure 2) that is not present in either m-ptase or fb-ptase. Alignment of these residues with sequences in the GenBank database showed a region of sequence similarity to the regulatory subunit of cAMP-dependent protein kinase. The significance of this homology is currently unknown as the function of this region of cAMP-dependent protein kinase has not been elucidated. The presence of this region on the surface of 1-ptase suggests that it may interact with some moiety to alter function. Deletional and mutational analysis of this region will likely provide insight regarding this speculation.

The metal binding/active site of 1-ptase is a large hydrophilic cavity located near the surface of the molecule. Proximal to the metal binding residues are THR 158, which is highly conserved in the DPIDST sequence motif, and LYS 37, which is located 3.05 Å from the threonine hydroxyl group. Site-directed mutation of THR 158[1] or LYS 37 (York et al., 1994a) shows that both are essential for catalytic activity. Threonine 158 does not directly bind metal, but it is located 2.86 Å from H_2O 45 which does coordinate both metal ions, and LYS 37 is capable of hydrogen bonding THR 158. A sulfate ion, present in the crystal structure of m-ptase (Bone et al., 1992), is in a position similar to H_2O 45 of the 1-ptase structure and is thought to occupy the same position as the 1-phosphate of the substrate in m-ptase (Pollack et al., 1994). We suggest that THR 158 participates in catalysis by either coordinating an activated water molecule or aligning the 1-phosphate of the substrate for nucleophilic attack.

The metal binding sites of 1-ptase are very similar to those of fb-ptase (Zhang et al., 1993) and m-ptase (Pollack et al., 1994). 1-Ptase binds two juxtaposed Mg^{2+} ions, located 3.88 Å apart, which are coordinated by several carboxylate groups contributed by four secondary structure elements. Equivalent residues in fb-ptase coordinate two metals located approximately 3.7 Å apart. Pollack and co-workers (1994) have recently suggested two, or possibly three, metal binding sites on the basis of crystallographic studies of m-ptase in the presence of only Mn^{2+} ions (Bone et al., 1994b). The presence of two metal binding sites in 1-ptase explains a previously puzzling result wherein 1-ptase activity was stimulated by Mg^{2+} cooperatively with a Hill coefficient of 1.9 despite the fact that the enzyme is a monomer (Inhorn & Majerus, 1987). Similarly, activation of m-ptase by Mg^{2+} also shows positive cooperativity having a Hill coefficient of 2.0 (Ganzhorn & Chanal, 1990; Leech et al., 1993)

[1] X. Zhang, P. W. Majerus, and J. D. York, manuscript in preparation.

although in this case cooperativity was thought to be due to interactions between subunits. The presence of two or more metal binding sites in each subunit of m-ptase and the analogous cooperativity of 1-ptase monomer suggest that there is cooperative binding of metal at the adjacent sites rather than between subunits.

The mechanism of catalysis of these three enzymes is likely to proceed via a common two-metal-site activation of water. ^{18}O-Labeled water exchange studies of fb-ptase (Domanico et al., 1985) and m-ptase (Leech et al., 1993) suggest that a metal-activated water molecule is responsible for nucleophilic attack of the phosphate ester bond, suggesting that the reaction does not proceed via a phospho-enzyme intermediate. The presence of two metal binding sites in the fb-ptase crystal structure led Zhang et al. (1993) to propose a catalytic mechanism wherein there is ordered binding of a first Mg^{2+} at site 1 and then substrate, followed by a second Mg^{2+} at site 2. Binding of the second metal ion is proposed to orient and activate a water molecule for subsequent in-line nucleophilic attack on the phosphate ester bond. Indirect evidence supporting this model comes from the dramatic movement of metal site 2 in the presence of Gd^{3+}. Gd^{3+} is a lanthanide metal having properties similar to those of Ca^{2+}. Ca^{2+} is a competitive inhibitor of 1-ptase with respect to Mg^{2+}, suggesting that it occupies identical sites (Inhorn & Majerus, 1988). The movement of metal site 2 to 4.88 Å away from H_2O 45 could prevent the necessary activation, which would explain Gd^{3+} inhibitory action. Recent crystallographic studies (Bone et al., 1994a,b) have led Pollack et al. (1994) to suggest that a similar two-Mg^{2+} activation mechanism of catalysis exists for m-ptase. The presence of two Mg^{2+} binding sites in 1-ptase suggests a similar mechanism, although we cannot conclusively define the reaction order. Furthermore, cocrystallization studies of 1-ptase with substrate in the presence of various metals will provide insight into the reaction order, substrate binding site, and mechanism of catalysis.

The observation that two metal binding sites are present in 1-ptase, fb-ptase, and m-ptase raises the possibility that the mechanism of uncompetitive Li^+ inhibition proceeds by competition for the second or yet a third metal site present when substrate is bound. Hallcher and Sherman (1980) showed that Li^+ is an uncompetitive inhibitor of m-ptase and that high concentrations of Mg^{2+} also act as an uncompetitive inhibitor. Ganzhorn and Chanal (1990) and Leech et al. (1993) demonstrated that inhibitory binding of Li^+ and Mg^{2+} are mutually exclusive, corroborating the idea that they utilize similar sites. Such a model has been proposed for m-ptase (Pollack et al., 1994) in which Li^+ binds to the enzyme–substrate complex at the second metal binding site. The same may also be true for fb-ptase since this enzyme is also potently inhibited by Li^+ (Marcus & Hosey, 1980), although the mode of inhibition in this case has not been determined. Our understanding as to the mechanism of lithium inhibition will be greatly enhanced by structural studies of these three proteins and ultimately may shed insight into our understanding of the mode of action of lithium used in the treatment of manic depressive disorders.

ACKNOWLEDGMENT

We thank Drs. Arthur Arnone, Robert Fletterick, Longyin Chen, and Scott White for helpful discussions and advice. We also thank Dr. Scott White and Dr. J. Evan Sadler for critical review of the manuscript.

REFERENCES

Agarwal, R. C. (1978) *Acta Crystallogr. A34*, 791–809.
Bansal, V. S., & Majerus, P. W. (1990) *Annu. Rev. Cell Biol. 6*, 41–67.
Berridge, M. J., & Irvine, R. F. (1989) *Nature 341*, 197–205.
Blundell, T. L., & Johnson, L. N. (1976) *Protein Crystallography*, Academic, New York.
Bone, R., Springer, J. P., & Atack, J. R. (1992) *Proc. Natl. Acad. Sci. U.S.A. 89*, 10031–10035.
Bone, R., Frank, L., Springer, J. P., Pollack, S. J., Osborne, S., Atack, J. R., Knowles, M. R., Mcallister, G., Ragan, C. I., Broughton, H. B., Baker, R., & Fletcher, S. R. (1994a) *Biochemistry 33*, 9460–9467.
Bone, R., Frank, L., Springer, J. P., & Atack, J. R. (1994b) *Biochemistry 33*, 9468–9476.
Brünger, A. T. (1988) *J. Mol. Biol. 203*, 803–816.
Cambillua, C., & Horjales, E. (1987) *J. Mol. Graphics 5*, 174–178.
Dingwall, C., & Laskey, R. A. (1991) *Trends Biochem. Sci. 16*, 478–481.
Domanico, P. L., Rahil, J. F., & Benkovic, S. J. (1985) *Biochemistry 24*, 1623–1628.
Gani, D., Downes, C. P., Batty, I., & Bramham, J. (1993) *Biochim. Biophys. Acta 1177*, 253–269.
Ganzhorn, A. J., & Chanal, M.-C. (1990) *Biochemistry 29*, 6065–6071.
Gee, N. S., Reid, G. G., Jackson, R. G., Barnaby, R. J., & Ragan, C. I. (1988) *Biochem. J. 249*, 777–782.
Hallcher, L. M., & Sherman, W. R. (1980) *J. Biol. Chem. 255*, 10896–10901.
Hamlin, R. (1985) *Methods Enzymol. 114*, 416–452.
Howard, A. J., Nielsen, C., & Xuong, Ng. H. (1985) *Methods Enzymol. 114*, 452–472.
Huheey, J. E. (1978) *Inorganic Chemistry*, 2nd ed., Harper and Row, New York.
Inhorn, R. C., & Majerus, P. W. (1987) *J. Biol. Chem. 262*, 15946–15952.
Inhorn, R. C., & Majerus, P. W. (1988) *J. Biol. Chem. 263*, 14559–14565.
Jones, T. A. (1985) *Methods Enzymol. 115*, 157–171.
Jones, T. A., Zuo, J.-Y., Cowan, S. W., & Kjeldgaard, M. (1991) *Acta Crystallogr. A47*, 110–119.
Kabsch, W., & Sander, C. (1983) *Biopolymers 22*, 2577–2637.
Ke, H., Thorpe, C. M., Seaton, B. A., Marcus, F., & Lipscomb, W. N. (1989) *Proc. Natl. Acad. Sci. U.S.A. 86*, 1475–1479.
Leech, A. P., Baker, G. R., Shute, J. K., Cohen, M. A., & Gani, D. (1993) *Eur. J. Biochem. 212*, 693–704.
Liang, J.-Y., Zhang, Y., Huang, S., & Lipscomb, W. N. (1993) *Proc. Natl. Acad. Sci. U.S.A. 90*, 2132–2136.
Majerus, P. W. (1992) *Annu. Rev. Biochem. 61*, 225–250.
Marcus, F., & Hosey, M. M. (1980) *J. Biol. Chem. 255*, 2481–2486.
Mathews, F. S., Levine, M., & Argos, P. (1972) *J. Mol. Biol. 64*, 449–464.
Neuwald, A. F., York, J. D., & Majerus, P. W. (1991) *FEBS Lett. 294*, 16–18.
Nishizuka, Y. (1986) *Science 233*, 305–312.
Pollack, S. J., Atack, J. R., Knowles, M. R., McAllister, G., Ragan, C. I., Baker, R., Fletcher, S. R., Iversen, L. L., & Broughton, H. B. (1994) *Proc. Natl. Acad. Sci. U.S.A. 91*, 5766–5770.
Read, R. J. (1986) *Acta Crystallogr. A42*, 140–149.
Silver, P. A. (1991) *Cell 64*, 489–497.

Sylvia, V. L., Curtin, G. M., Noran, J. O., Stec, J., & Busbee, D. L. (1988) *Cell 54*, 651−658.
Terwilliger, T. C., Kim, S. H., & Eisenberg, D. (1987) *Acta Crystallogr. A43*, 1−5.
Xuong, Ng. H., Nielsen, C., Hamlin, R., & Anderson, D. (1985) *J. Appl. Crystallogr. 18*, 342−355.
York, J. D., & Majerus, P. W. (1990) *Proc. Natl. Acad. Sci. U.S.A. 87*, 9548−9552.
York, J. D., Veile, R. A., Donis-Keller, H., & Majerus, P. W. (1993) *Proc. Natl. Acad. Sci. U.S.A. 90*, 5833−5837.
York, J. D., Saffitz, J. E., & Majerus, P. W. (1994a) *J. Biol. Chem. 269*, 19992−19999.
York, J. D., Chen, Z., Ponder, J. W., Chauhan, A. K., Mathews, F. S., & Majerus, P. W. (1994b) *J. Mol. Biol. 236*, 584−589.
Zhang, K. Y. J. (1993) *Acta Crystallogr. D49*, 213−222.
Zhang, K. Y. J., & Main, P. (1990) *Acta Crystallogr. A46*, 377−381.
Zhang, Y., Liang, J.-Y., & Lipscomb, W. N. (1993) *Biochem. Biophys. Res. Commun. 190*, 1080−1083.